

# COMPUTATION OF A DYNAMICALLY DEPLOYED FLAP EMPLOYING ADAPTIVE BODY RECOVERY

**J. J. Roper, J. A. Edwards**  
**DERA Fort Halstead, Sevenoaks, Kent, UK**

**Keywords:** *Dynamic, Adaptive, Unsteady, Computation*

## Abstract

*This paper examines the effectiveness of the adaptive body recovery technique[3][4] for computing separated hypersonic flows. The Baldwin-Lomax algebraic turbulence model was added to the code and modified, through under-relaxation of the turbulent viscosity to effect transition from laminar to turbulent flows over various distances, in order to match experimental data for a series of transitional separated flows. This turbulence model was then employed, in conjunction with the moving body boundary conditions, to predict the lag in separation growth with flap angle for a rapidly deployed flap. Agreement between the computational and experimental dynamic angular lag was found to be good.*

## Nomenclature

c	Reference length
P	Pressure
Re	Reynolds number
T	Temperature
u	Streamwise velocity
$\chi$	Intermittency function
$\mu$	Viscosity
$\rho$	Density
$\omega$	Angular rate

## Subscripts:

$\infty$	Freestream
0	Stagnation
t	Turbulent
x	Based on length

## 1 Introduction

Computation of unsteady, dynamic flows over temporally varying geometries, whilst of significant interest to aerodynamicists (for example moveable control surfaces) can present difficulties for computational prediction. The two main difficulties are: the need to provide automatic meshing algorithms (to cope with body movement and/or shape change) and the derivation and implementation of boundary conditions appropriate to moving/deforming surfaces. The latter becomes particularly problematic when computing turbulent flows for which the turbulence is modelled using non-algebraic turbulence models.

A technique was derived, implemented and demonstrated, by which flows around arbitrarily moving and/or deforming geometries can be readily computed in a highly efficient automated manner exploiting adaptive mesh refinement[1]. These extensions were implemented within the DRA Adaptive Mesh Refinement code (DRAMR) which provides an environment for obtaining solutions to systems of non-linear partial differential equations using hierarchical mesh refinement[2]. Hierarchical mesh refinement is achieved by automatic refinement of patches of cells (by subdivision) to produce a hierarchy of progressively refined solutions, with adaption triggered by user specified criteria (typically spatial flowfield gradients). A schematic showing two levels of 2x2 mesh refinement is given in Figure 1.

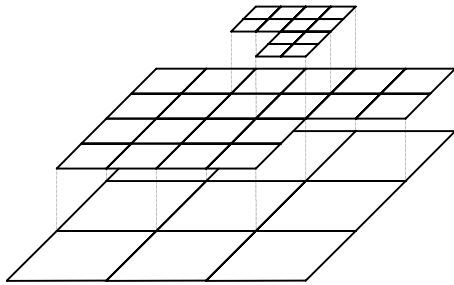


**Figure 1. Schematic Showing Two Levels of 2x2 Mesh Refinement**

The efficiency of the moving body extensions to DRAMR stems, in part, from exploitation of adaptive mesh refinement, and avoiding generating small cells (which results in reduced timesteps). These extensions enable automatic meshing of arbitrary body surfaces and provide conservative boundary conditions for dynamically moving surfaces. An illustration of an automatically meshed aerofoil section is given in Figure 2.

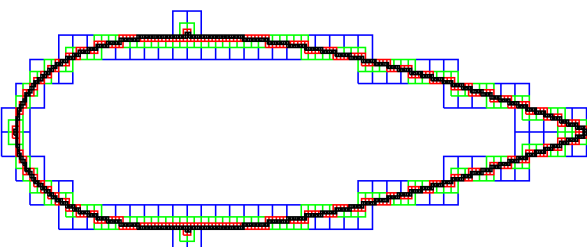


**Figure 2. Mesh Adaption Used To Capture The Boundary of a NACA 65-009 Aerofoil**

These extensions are thoroughly documented in references [3] and [4]. Validation of these techniques was by comparison between computational and experimental data for static body flows (automatically meshed), and a dynamic constrained body motion. The computed dynamic motion was compared with predictions based on experimental data. Both static and dynamic agreement was seen to be good, however, the body motion used to assess the technique's dynamic capabilities was quasi-steady, and hence the ability to predict rapidly moving surfaces (with dynamic flowfields) had not been demonstrated.

This paper presents computations and comparison with experiment[5] for a rapidly

deployed flap ( $\approx 3000^{\circ}\text{s}^{-1}$ ). This motion was shown (experimentally) to be dynamic in nature and show a dynamic lag in flow separation consistent with its rapid motion. The reduced angular frequency of the flap deployment ( $\omega c/2u$ ) is  $\approx 1.3 \times 10^{-3}$ , from which the flow might be expected to be quasi-steady, however assessing steadiness on the basis of reduced angular frequency assumes the flow to be inviscid. It is believed that this flow exhibits dynamic effects due to the presence of the large viscous separated region present within the flowfield.

## 2 Static Transitional Ramp Flows

A series of static and dynamic experiments were performed by Smith[5] at Southampton University using a Mach 6.85 isentropic light piston compression tube wind tunnel. The flow conditions were:

$$\begin{aligned} Re_\infty &= 2.45 \times 10^6 \text{ m}^{-1} & P_0 &= 552000 \text{ Nm}^{-2} \\ T_\infty &= 58.74 \text{ K} & P_\infty &= 153.0 \text{ Nm}^{-2} \\ \rho_\infty &= 0.00876 \text{ kg m}^{-3} & u_\infty &= 1070.0 \text{ ms}^{-1} \\ \mu_\infty &= 3.83 \times 10^{-6} \text{ kg m}^{-1} \text{ s}^{-1} \end{aligned}$$

The model geometry comprised a flat plate (155mm in length) with a flap attached at the trailing edge (51mm in length) as illustrated in Figure 3 (together with a schematic of a separated flowfield).

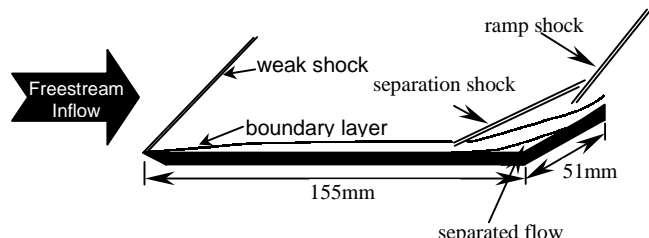


**Figure 3. Schematic of Hypersonic Flat Plate-Flap Flowfield**

Experimental data are available[5] in the form of schlieren images and heat transfer measurements for various static and dynamic configurations. Without the flap deployed, the flowfield over the entire model is laminar, whilst as the flap angle is increased, the flow appears to undergo transition in the free shear

layer, probably leading to turbulent reattachment[16]. Flowfield unsteadiness was not observed in any of the static flap cases.

Smith[5] presents results at various freestream Reynolds numbers to attempt to quantify the effects of transition. In Smith's preliminary discussion of the static flap flows, it is suggested that the flow is laminar across the full range of flap angles ( $0^\circ$ - $40^\circ$ ) at the lowest Reynolds number flow ( $Re_\infty=2.45 \times 10^6 m^{-1}$ ). In subsequent discussions it was acknowledged that the flow might not be laminar at all of the flap angles. For a plate of length 0.206m (flap angle = zero), the flow is likely to be laminar throughout the flowfield ( $Re=504,700$  over the length of the plate, typically  $Re_c \approx 500,000$ ). As the flap angle is increased the flow will undergo transition and thus a turbulence model was required to predict the flow over the full range of flap angles that were examined experimentally.

An advantage of zero equation turbulence models is that they simply postprocess computational flowfields to infer a turbulent viscosity based on the flowfield data, and hence no special considerations are necessary to accommodate moving body surfaces. As the stationary computations presented here were a pre-cursor to the dynamic cases, it was desirable to employ the same turbulence model for both (to enable direct comparison of corresponding static and dynamic flap deployments).

A non-dimensional form of the Baldwin Lomax[7] turbulence model consistent with the hierarchical mesh refinement and numerics employed by DRAMR was produced and implemented. Formulation and application of the Baldwin-Lomax turbulence model was identical to that applied by Baldwin and Lomax for their supersonic compression ramp flow[7]. Comparison of computational solutions produced by DRAMR and a commercial CFD code[13] showed identical results.

Due to the potential complexity of performing automatic spatial refinement with

adaption on the basis of flowfield spatial gradients, simultaneous with ensuring sufficient mesh refinement to recover the body surface and to capture the boundary layer, spatial flowfield gradient adaption was disabled. This resulted in a significant increase in computational cost, as a sufficiently fine baseline mesh had to be used throughout, even where such refinement was unnecessary. Fortunately the cost of undertaking these computations, whilst high, was not prohibitive and the luxury of over-refinement could be accommodated.

Since the flow is (dependent on location and flap angle) laminar, transitional or turbulent, a computational mesh was required for which mesh convergence could be established for all of these flow regimes. Preliminary laminar and turbulent computations were performed to assess mesh convergence. Meshes which were sufficient for the turbulent computations were also sufficient for the laminar computations (the requirements for the turbulent meshes were more acute than for the laminar meshes, and hence the turbulent meshes were over-specified for the laminar flows) and hence mesh convergence was concentrated on the turbulent flows. It was established that with the exception of minor perturbation to the last two or three grid points on the flap, the wake flow was unimportant for these computations.

Experimental results[5] are reconstructed in Figure 4 together with the results of the preliminary computations, highlighting that the experimental results lie between the fully laminar and the fully turbulent computations. The results of these turbulent computations are consistent with previous investigations into incipient separation[12].

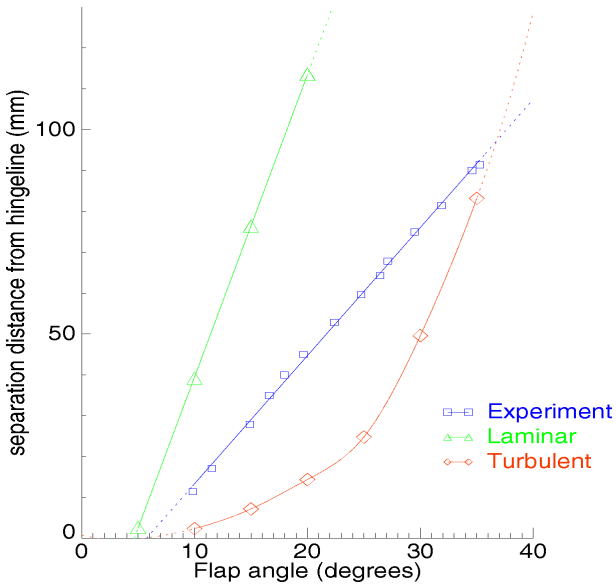


**Figure 4. Comparison of Separation Locations (experimental and computational)**

Separation of the flow is seen at flap angles of 5° and above computationally and 6° and above experimentally. This compares favourably with predictions of the onset of laminar separation of 5°[8][9][10][11][12]. A typical flowfield, including underbody and wake flows is presented in Figure 5 (for a fully turbulent 30° flap flow).

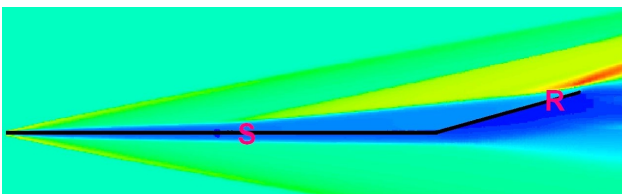


**Figure 5. Turbulent Mach 6.85 Flowfield Over A Flat Plate and 30° Flap (Density)**

Due to concerns regarding accurate determination of experimental location of separation when using optical techniques, the methods by which the separated length was determined were examined. It is known that estimating the location of separation by visual means (for example, by examination of schlieren images) can produce large errors, especially for flows with thick boundary layers and/or high Mach numbers (due to the reduced angle of the separation shock to the freestream). Whilst this boundary layer is relatively thin,

errors can still be significant. Figure 6 shows a computational flowfield which is shaded according to absolute density gradient. It is seen that if one assumes that separation occurs where the projected separation shock would impinge the wall, a significant error would result (in this case an error of 18.2mm or 24% of the correct separated length).

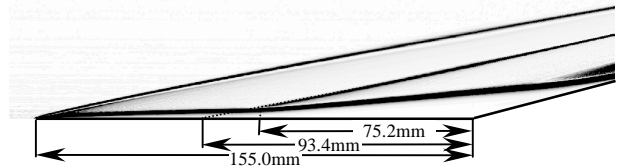


**Figure 6. Absolute Density Gradient (25° Flap)**

Smith obtained separation lengths by projecting normal to the wall at the furthest upstream occurrence of the separation shock (“separation location has been taken as the intersection of the separation shock with the visible edge of the boundary layer”[5]). It is seen from Figure 6, that this should yield acceptably accurate results.

Various techniques were examined to attempt to replicate the static data of Smith whilst retaining the simple zero equation turbulence model of Baldwin and Lomax. Since the experimental data falls between the fully laminar and fully turbulent (and the flowfield is recognised as being transitional) various techniques to modify the spatial extent over which the flow was being modelled as laminar and turbulent were examined. This, in no way, was intended to model the complex processes of flow transition, and was simply to provide agreement between static computational and experimental data for the purposes of quantifying the performance of the adaptive body recovery techniques when predicting dynamic moving body flows. The numerical relaxation methods examined included:

- Instantaneous transition at the hingeline (Figure 7a),
- Instantaneous transition at separation (Figure 7b),

- Laminar at separation, fully turbulent at reattachment – fixed (Figure 7c),
- Laminar at separation, fully turbulent at reattachment – floating (Figure 7d),
- Laminar at separation, becoming turbulent over  $\Delta Re_\infty = 125,000$  (Figure 7e),
- Laminar at separation, becoming turbulent over  $\Delta Re_\infty = 250,000$  (Figure 7e),
- Laminar at separation, becoming turbulent over  $\Delta Re_\infty = 500,000$  (Figure 7e).

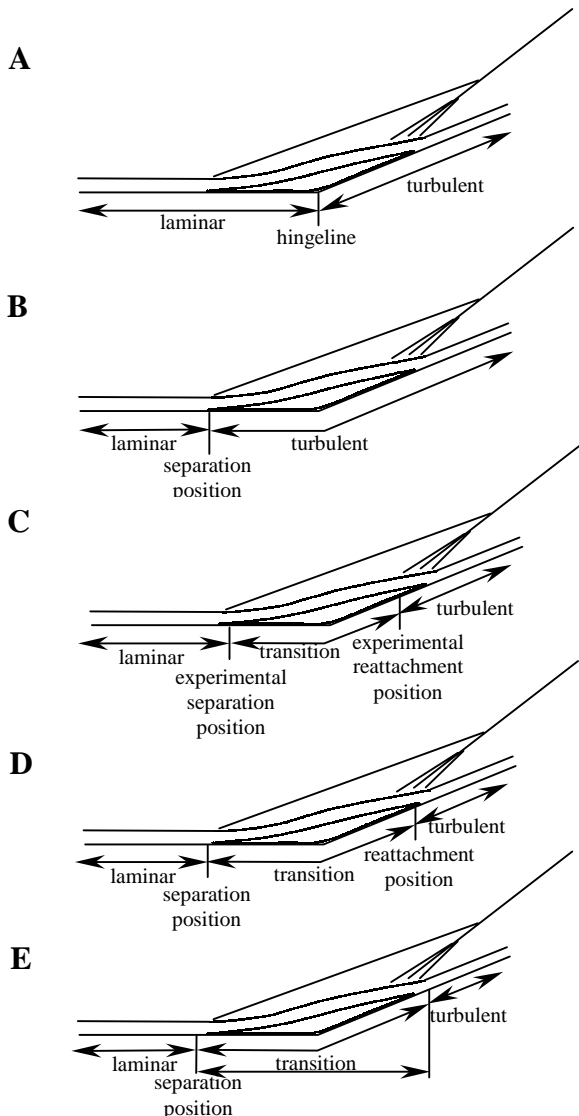


**Figure 7. Turbulent Viscosity Under-Relaxation Schemes Examined.**

Whilst instantaneous transition is readily achieved (setting  $\mu_t=0.0$  upstream of transition), transition of the flow over a finite distance requires implementation of an intermittence

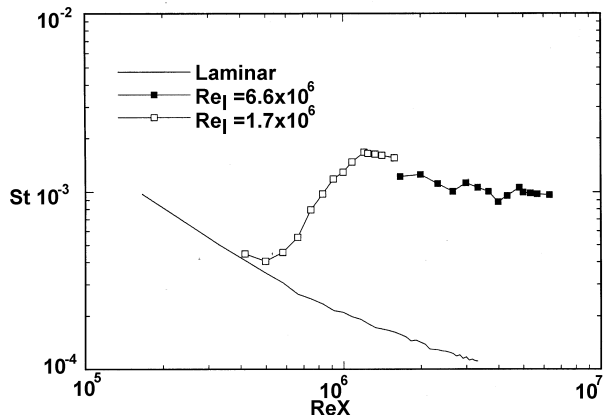
function to scale the turbulent viscosity at every streamwise location. To cast this in computational terms and to enforce laminar and turbulent flows where required, an under relaxation factor  $\chi$  is used to scale the turbulent viscosity  $\mu_t$ . This is similar to the method suggested by Dhawan and Narasimha[14]. Rather than use an arbitrarily contrived profile for transition, an experimental profile was imposed.

Figure 8 presents variation in Stanton number with Reynold's number for laminar, turbulent and transitional flow over an elliptic cone[15]. Sampling this data and fitting the results with a polynomial produces a variation in  $\chi$  with  $Re_x$  which was included in the Baldwin Lomax turbulence model.

The polynomial fit is given by:

$$\chi = 0.01469 + 0.08472\bar{x} + 2.3151\bar{x}^2 - 1.4226\bar{x}^3$$

where,  $\bar{x} = \frac{Re_x - 417000}{795000}$  (i.e.  $0 \leq \bar{x} \leq 1$  over the transition region),



**Figure 8. Variation in Stanton Number Over an Elliptic Cone With Reynolds Number**

In this manner a fixed (or floating) point is selected as the location at which transition is to commence and a solution produced with laminar, transitional and fully turbulent flows as required.

Results obtained using these techniques are presented in Figure 9.

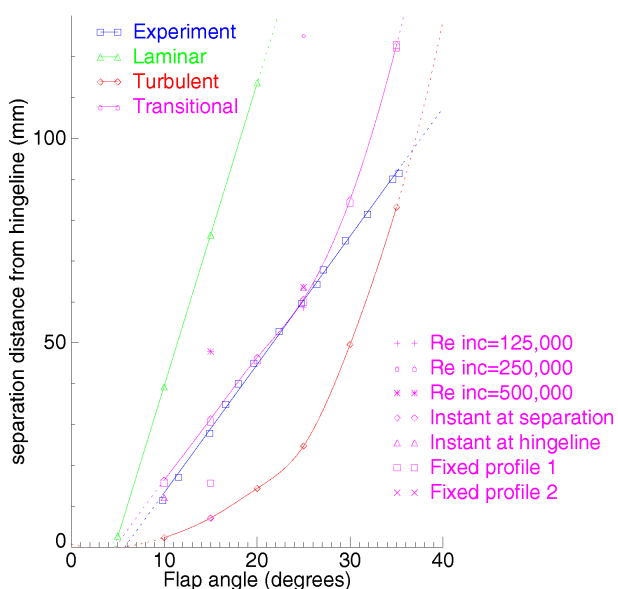


**Figure 9. Variation in Separation Position – Experiment and Computation**

A typical transitional flowfield produced using adaptive body recovery ( $\Delta Re_{\infty}=250,000$  with  $15^\circ$  flap deployment) is presented in Figure 10 from which it is seen that the flow does not depart significantly in qualitative terms from that which might be expected for either a fully laminar or a fully turbulent flow.

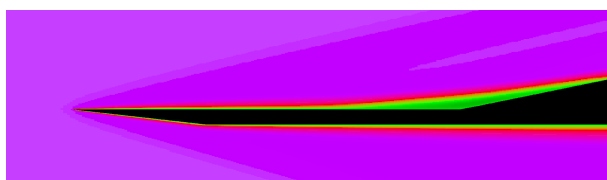


**Figure 10. Typical Transitional Flow (15° Flap Deployment,  $\Delta Re=250,000$ , Pressure)**

Using this technique we find that small flap angle flows are fully laminar, and that larger flap angle flows are transitional or fully turbulent. Experimental and computational variation in separation position with flap angle is given in Figure 9, and reasonable agreement is seen for angles up to  $\approx 25^\circ$  with the  $\Delta Re_{\infty}=250,000$  model. It has been suggested that the experimental data of Smith was influenced by additional 3D effects caused by lateral spillage, or by shock boundary layer interaction induced effects on the side plates, and that the larger flap angles will exhibit the largest effects [16]. This may, in part, account

for some of the deviation between experiment and computation, which is evident in Figure 9.

### 3 Dynamically Deployed Flap

Kuehn[17] discovered that for supersonic slowly moving ramps there was no evidence of hysteresis and moreover the instantaneous flowfield for a specific ramp angle was identical to its static counterpart. This is only true for relatively slowly moving surfaces i.e. where the flowfield is quasi-steady. Smith[5] showed that for a rapidly deployed flap.

Using the technique of adaptive body recovery, the flow over a rapidly deployed flap was computed. Preliminary computations were performed to ensure that sufficient baseline mesh resolution had been achieved and that the solutions to the static cases with the under-relaxed Baldwin-Lomax turbulence model were producing the same results with adaptive body recovery as those produced with conventional body fitted grids. Subsequent to these validations, full dynamic computations were performed. An initial flat plate flow (flap deployment angle = zero) was generated as the starting condition for computation of the ensuing motion.

The experimental flap position and velocity histories for the flap deployment are given in Figures 11 and 12[5].

To provide a smoothly varying flap motion for the computations, these data were sampled and fitted with cubic splines prior to input to the computation. To ensure consistency, the angular positional history was produced by integration of the angular velocity history.

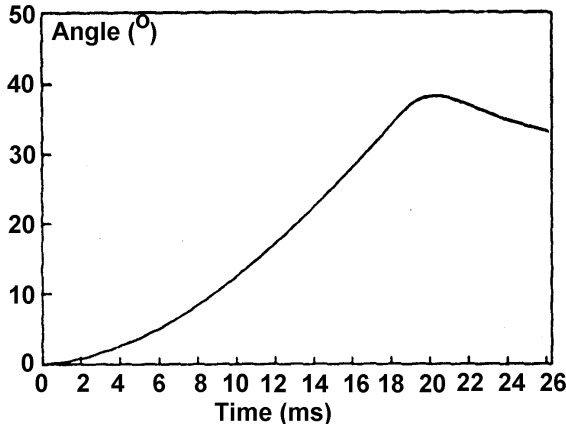


Figure 11. Experimental Variation in Flap Angle With Time[5]

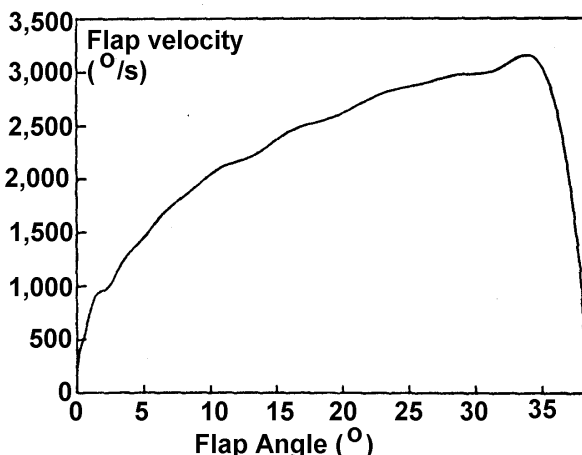


Figure 12. Experimental Variation in Flap Angular Velocity With Time[5]

Determining which cells are undergoing creation or destruction (exposure and occlusion by the body) was performed by comparing two body positions at each iteration and locating cells whose positional status (inside, outside, or boundary) had changed. To ensure optimal accuracy, the following temporal body placement scheme was implemented.

- i. Set the initial body angle according to the profile in Figure 11 (based on the physical time elapsed from the start of the body motion),
- ii. Set the initial angular body rate according to Figure 12,
- iii. Compute the time step (subject to the CFL condition),

- iv. Set the angular increment according to (ii) and (iii),
- v. Set the final angular position according to (i) and (iv).

In this manner the flap prescribes exactly the same motion as in the experiment. Minute errors are in evidence between the predicted angular position and angular rate at the end of an iteration, and the new values computed at the beginning of the next (due to the size of the time step and the magnitude of the angular acceleration these are small). Positional errors are typically of the order of  $10^{-6}\%$  and since the positional errors are due to extrapolation of linearised angular velocities, the errors in angular velocity must be similarly small.

To produce a converged flat plate solution (laminar) prior to the flap deployment, and to prevent spurious application of the turbulence model (due to the formation of tiny localised separated regions during the numerics of the computation starting), the turbulent viscosity is set to zero throughout the domain prior to convergence being attained. In this manner the computation progresses to a converged steady laminar flat plate flow from which the flap is released and the transitional turbulence model will engage as soon as separation occurs.

Initial computations employing a hinged flat plate-flap configuration (as per the experimental configuration), experienced numerical difficulties due to the dynamically strengthening expansion on the underside of the flap. It has been shown previously that the wake flow need not be modelled in order to accurately predict the flow over the flap, and hence this problem was avoided by utilising the innate ability of the code to model flows over arbitrarily deforming geometries. Body rotation was replaced by iterative reconstruction of the body surface so that at each time-step the entire surface of the flat plate and the flap were recreated, with the underside of the flat plate extended to create a flat plate-wedge configuration (seen later in Figure 15) (the

computational overhead for this was insignificant).

Since the static experimental and computational separated lengths differ at the larger incidences (Figure 9), for the purposes of assessing dynamic separation lag, the difference between the computational static and computational dynamic results are presented.

Figure 13 presents the dynamic lag in length terms (normalised with respect to flap length) for both the experiment and the computation. It is seen that although the onset of dynamic lag is well-predicted ( $\approx 20^\circ$ ), the magnitude of the lag in length terms is not. This was expected, and is attributed to the over-prediction in separated length by the turbulence model at higher incidences (Figure 9).

Presenting the dynamic lag in angular terms (as per Smith[5]), whereby the angular lag is defined as the difference between the dynamic flap angle and the steady flap angle required to produce the same separation position, overcomes this comparative difficulty. This is illustrated in Figure 14 and it is seen that agreement between the experimental and computational angular lag is good.

The computed peak angular lag appears to be approximately  $5^\circ$ , which compares favourably with the experimentally determined lag of  $6^\circ$ .

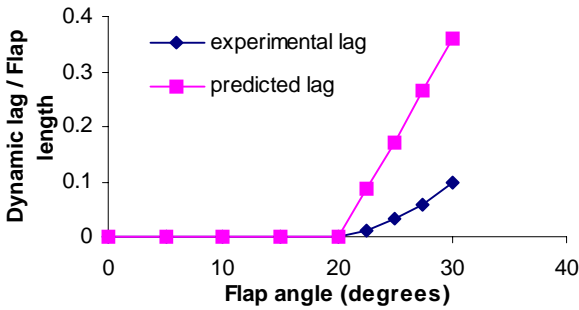


Figure 13. Dynamic Lag With Flap Angle (In Length Terms)

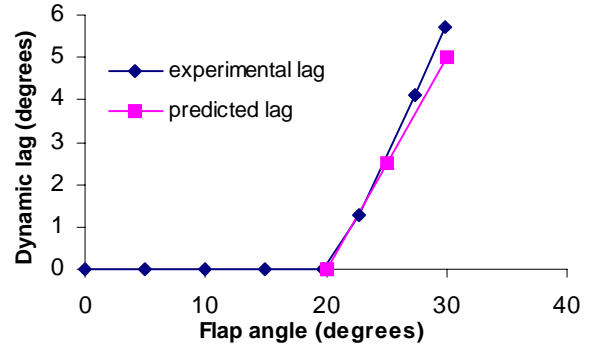


Figure 14. Dynamic Lag With Flap Angle (In Angular Terms)

Sample instantaneous density plots during the course of flap deployment are presented in Figure 15. The colour range for all of the plots in Figure 15 is fixed to enable direct comparison ( $0 \leq \rho/\rho_\infty \leq 10$ ).

To demonstrate temporal convergence the computations were repeated with the timestep halved. Identical results were produced for the variation in separation and reattachment positions with time and hence temporal convergence was assured.

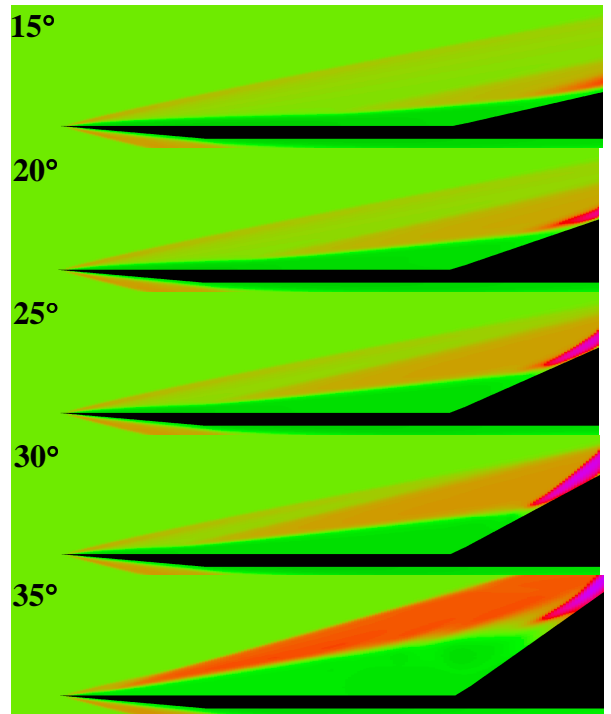


Figure 15. Dynamic Computational Flowfields (density)

## 4 Conclusions.

Separated flows were successfully computed with the adaptive body capture code, and incipient separation found to be in good agreement with both experiment and theory.

Experimental static data for several flat plate flap flows were modelled using an under-relaxed Baldwin-Lomax turbulence model (to match experimental transitional flows – not as a model of the process of transition) and quantitative and qualitative agreement found to be good for flap angles between 0° and 25°.

Experimental flap deployment profiles were employed, in conjunction with a deforming body surface and the transitional adaptive body capture code, to predict the development of a separated region during the course of rapid flap deployment. A lag in separation position was observed and found to be in reasonable agreement with experimental data.

## 5 References.

- [1] Berger, M J, "Adaptive Mesh Refinement for Hyperbolic Partial Differential Equations", PhD Thesis, Stanford University, 1982.
- [2] Quirk, J J, "An Adaptive Grid Algorithm For Computational Shock Hydrodynamics." Phd Thesis, Cranfield University , 1991
- [3] Edwards, J A, Roper, J J, "Dynamic Moving Body Flow Computations With DRAMR", March 1998, DERA/WSS/WX5/TR980312/1.0
- [4] Edwards, J A, Roper, J J, "Adaptive Moving Body Flow Computations", AIAA Paper 99-0393, 37th AIAA Aerospace Sciences Meeting and Exhibit, January 11-14, 1999, Reno, NV.
- [5] Smith, A J D, "The Dynamic Response of a Wedge Separated Hypersonic Flow and its Effects of Heat Transfer", PhD Thesis, Southampton University, 1993
- [6] Dolling, D S, "Fluctuating Loads in Shock Wave/Turbulent Boundary Layer Interaction: Tutorial and Update." AIAA 93-0284
- [7] Baldwin, B S, Lomax, H, "Thin-Layer Approximation and Algebraic Model for Separated Turbulent Flows", AIAA 78-257, Huntsville, AL
- [8] Coleman, G T, Stollery, J L, "Incipient Separation of Axially Symmetric Hypersonic Turbulent Boundary Layers", AIAA Journal, Vol. 12, No. 1, January 1974, pp. 119-120
- [9] Needham, D A, Stollery, J L, "Hypersonic Studies of Incipient Separation and Separated Flows", ARC 27752,1966.
- [10] Kuehn, D M, "Laminar Boundary Layer Separation Induced by Flares on Cylinders with Highly Cooled Boundary Layers at a Mach Number of 15", NASA TN D-2610, 1965.
- [11] Kuehn, D M, "Laminar Boundary Layer Separation Induced by Flares on Cylinders at Zero Angle of Attack", NASA TR-R-146, 1962.
- [12] Edwards, J A, Roper, J J, "A Computational Investigation of the Incipient Separation of a Hypersonic Turbulent Boundary Layer", AIAA 97-0769, 35th Aerospace Sciences Meeting and Exhibit, Jan, 1997, Reno, NV.
- [13] Sale, N M, "SPIKE v2 User Guide", TN 14/94, Fluid Gravity Engineering Ltd., February 1994
- [14] Dhawan, S, Narasimha, R, "Some Properties of Boundary Layer Flow During Transition from Laminar to Turbulent Motion", Journal of Fluid Mechanics, Volume 3, 1958.
- [15] Kimmel, R, Poggie, J, "Transition on an Elliptic Cone at Mach 8", Presented at 23rd TTCP WTP-2 Meeting, 27th April – 1st May 1998, DERA Bedford and DERA Fort Halstead.
- [16] Private communication. R East, Southampton University, December 1998.
- [17] Kuehn, D M, "Turbulent Boundary Layer Separation Induced by Flares on Cylinders at Zero Angle of Attack", TR R-117, 1961, NASA